

Available online at [www.sciencedirect.com](http://www.sciencedirect.com)

SciVerse ScienceDirect

journal homepage: [www.elsevier.com/locate/ije](http://www.elsevier.com/locate/ije)

# Dehydrogenation of pure and Ti-doped Na<sub>3</sub>AlH<sub>6</sub> surfaces from first principles calculations

Monica Pozzo<sup>a,b,\*</sup>, Dario Alfè<sup>a,b,c,d</sup>

<sup>a</sup> Department of Earth Sciences, University College London, Gower Street, London WC1E 6BT, United Kingdom

<sup>b</sup> Thomas Young Centre@UCL, University College London, Gower Street, London WC1E 6BT, United Kingdom

<sup>c</sup> Department of Physics and Astronomy, University College London, Gower Street, London WC1E 6BT, United Kingdom

<sup>d</sup> London Centre for Nanotechnology, University College London, 17-19 Gordon Street, London WC1H 0AH, United Kingdom

## ARTICLE INFO

### Article history:

Received 9 April 2011

Received in revised form

6 September 2011

Accepted 11 September 2011

Available online 5 October 2011

### Keywords:

Sodium alanates

Titanium catalyst

Hydrogen absorption

First principles calculations

## ABSTRACT

We have studied the dehydrogenation properties of pure and Ti-doped Na<sub>3</sub>AlH<sub>6</sub> surfaces using density functional theory. For the clean surface dehydrogenation is a multistep process, and involves the desorption of AlH<sub>4</sub> complexes which disrupt the structure of the surface. By doping the system with Ti, we found that the segregation energy of Ti is negative, therefore favoring localization of the impurity to the surface of Na<sub>3</sub>AlH<sub>6</sub>. Here Ti doping is shown to kinetically favor H<sub>2</sub> desorption, by reducing the energy barrier that the molecule needs to climb to leave the surface.

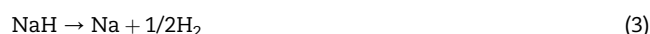
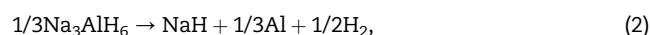
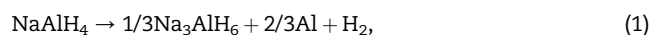
Copyright © 2011, Hydrogen Energy Publications, LLC. Published by Elsevier Ltd. All rights reserved.

## 1. Introduction

Sodium alanates have long been recognized as promising candidates for hydrogen storage purposes (see Sakintuna et al. [1] for a review and references therein). Among them, NaAlH<sub>4</sub> appeared appealing, having a theoretical H storage capacity of 7.5 wt% and low cost. However, irreversibility and poor kinetics precluded it as a possible on-board hydrogen storage material. This changed when Bogdanovic and Schwickardi [2] showed experimentally that by doping it with a transition metal catalyst – especially Ti – the processes of H absorption and desorption can be made reversible, and their kinetics improved under moderate conditions of temperature and pressure. The dehydrogenation kinetics of NaAlH<sub>4</sub> was also found to be further enhanced by improving the procedure used to dope the alanate with Ti [3]. However, although much

work has been devoted to it (see Jensen and Gross [4] for a review), the hydrogenation/dehydrogenation kinetics in NaAlH<sub>4</sub> has not yet reached satisfactory levels. The search for an appropriate doping metal capable of meeting this target is still open, both theoretically and experimentally.

The dehydrogenation of NaAlH<sub>4</sub> occurs in three steps:



The first two reactions occur at temperatures of 353 and 423 K, and release a total of 5.6 wt% of hydrogen. The third

\* Corresponding author. Department of Earth Sciences, University College London, Gower Street, London WC1E 6BT, United Kingdom.

E-mail address: [m.pozzo@ucl.ac.uk](mailto:m.pozzo@ucl.ac.uk) (M. Pozzo).

0360-3199/\$ – see front matter Copyright © 2011, Hydrogen Energy Publications, LLC. Published by Elsevier Ltd. All rights reserved.

doi:10.1016/j.ijhydene.2011.09.036

reaction releases the last 1.9 wt% of hydrogen at nearly 700 K, and because of this high dehydrogenation temperature it is not considered to be useful for practical applications.

Due to its role in the decomposition of  $\text{NaAlH}_4$ , much interest has been given to sodium aluminum hexahydride (hexahydride from now on),  $\text{Na}_3\text{AlH}_6$ . Besides being formed during decomposition of  $\text{NaAlH}_4$  upon dehydrogenation, it can also be synthesized by a direct process upon hydrogenation of Na and Al atoms [5]. In fact, even though  $\text{Na}_3\text{AlH}_6$  has a much lower theoretical H storage capacity than  $\text{NaAlH}_4$  (2.96 versus 5.6 wt% of H), the hydrogenation process (at about 200 °C or less) takes place at much lower H pressures (40–60 bar, instead of 130–150 bar for  $\text{NaAlH}_4$ ) [2], making it more appealing for possible future commercial purposes. Furthermore, after Ti doping,  $\text{Na}_3\text{AlH}_6$  can reversibly store and release hydrogen at a lower temperature and faster kinetics than  $\text{NaAlH}_4$ ; the dehydrogenation, storage capacity and cycling stability are also improved with respect to the undoped  $\text{Na}_3\text{AlH}_6$  sample [2].

Zidan et al. [6] showed experimentally that Zr is better than Ti for dehydrogenation of  $\text{Na}_3\text{AlH}_6$ , although Ti is better for the dehydrogenation of  $\text{NaAlH}_4$  from which  $\text{Na}_3\text{AlH}_6$  is formed. They therefore suggested a tandem doping technique of  $\text{NaAlH}_4$  to be achieved with both Zr and Ti simultaneously, in order to have positive effects in both directions of the hydrogenation/dehydrogenation processes. However, this is not a necessary requirement, giving that  $\text{Na}_3\text{AlH}_6$  obtained with mechanical alloying exhibits faster kinetics than the hexahydride obtained from the decomposition of  $\text{NaAlH}_4$  [7]. It was also found that Ce-doped  $\text{NaAlH}_4$  is characterized by fast kinetics and a stable hydrogen storage capacity around 4.7 wt% of  $\text{H}_2$ , compared to Ti-doped Na alanate [8]. Interestingly, it was found that dopants could form clusters on the alanate, and it was shown that small  $\text{Ti}_{13}$  clusters ball milled with  $\text{NaAlH}_4$  resulted in enhanced hydrogen exchange kinetics [9]. Another example of Ti-enhanced kinetics of absorption is that of Ti-doped Mg, where the presence of the transition metal helps hydrogen intake by lowering the  $\text{H}_2$  dissociation barrier [10].

A large number of theoretical studies have been done on the crystal structure, lattice parameters and electronic properties of  $\text{Na}_3\text{AlH}_6$  [11–21]. Overall, the structural parameters derived with theoretical calculations are in agreement with those found experimentally [14,22,23]. However, just a few theoretical papers have dealt with a Ti-doped sample [18–20]. Hydrogen diffusion in pure and Ti-doped  $\text{Na}_3\text{AlH}_6$  was studied by Voss et al. [20], who reported a combined theoretical–experimental work showing promotion of diffusion by Ti doping.

To our knowledge, all previous works on pure and doped  $\text{Na}_3\text{AlH}_6$  focused on bulk properties. However, dehydrogenation of the hexahydride is most likely affected by the behavior of its surfaces. In this work we therefore explicitly investigate the properties of both pure and Ti-doped  $\text{Na}_3\text{AlH}_6$  (010) surfaces, and we show the effect that Ti has on the geometry, the electronic structure and the desorption energy of hydrogen from the surface. We find that the electronic structure of the surface is not very different from that of the bulk, and this is true both for the pure and the doped system. However, our calculations show that the stability of the

Ti-doped hexahydride is higher than previously reported, as it is stabilized by the existence of a magnetic moment on the Ti atom not considered in previous studies. A study of the desorption mechanism shows that the presence of Ti reduces the energy barrier to  $\text{H}_2$  desorption, thereby improving the kinetics of the dehydrogenation process.

The paper is organized as follows. In Section 2 we briefly describe our first principles method of choice. Section 3 contains our results, and it is divided in subsections 3.1 and 3.2 which contain results of the pure  $\text{Na}_3\text{AlH}_6$  and Ti-doped  $\text{Na}_3\text{AlH}_6$  systems respectively, and subsection 3.3 which describes the electronic structure of the two systems. Conclusions follow in Section 4.

## 2. Techniques

The calculations are performed using density functional theory with the exchange-correlation functional of Perdew, Burke and Ernzerhof [24] (PBE) and the local density approximation (LDA). The interactions between the electrons and the nuclei are described with the projector-augmented-wave (PAW) formalism [25,26], as implemented in the VASP code [27]. We used 2p, 3s valence states for Na; 3s, 3p for Al; and 1s

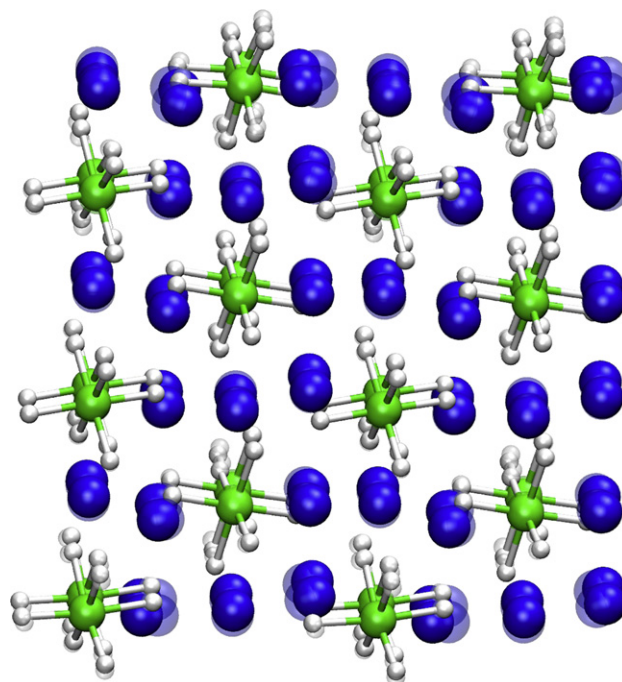


**Fig. 1** – Relaxed  $\text{Na}_{72}\text{Al}_{24}\text{H}_{144}$  slab. Na, Al and H atoms are shown as blue (dark gray), green (light gray) and small white balls respectively. Also shown are the corresponding positions in the bulk (shadowed balls). Surface relaxation is evident in the first layer, and quickly decays away in the deeper layers. The surface is perpendicular to the y direction, oriented almost vertically in the plane of the figure (slightly tilted towards the observer). (For interpretation of the references to color in this figure legend, the reader is referred to the web version of this article.)

for H. The plane wave cutoff was 324.5 eV. An efficient charge density extrapolation was used to speed up the calculations [28]. More specific, simulation dependent details are provided in the following sections.

Figs. 1 and 5 have been made using the VMD software [29].

### 3. Results

#### 3.1. Pure $\text{Na}_3\text{AlH}_6$

##### 3.1.1. Bulk properties

$\text{Na}_3\text{AlH}_6$  has a monoclinic structure (see Fig. 1), with space group symmetry  $P2_1/n$  ( $n$  14) and a primitive cell containing 20 atoms, i.e., 2 formula units (f.u.). Crystal structure parameters were optimized allowing for both atomic coordinates and cell shape to change. Energy versus volume curves were fitted to a Birch–Murnaghan equation of state [30]. Bulk structural properties of pure  $\text{Na}_3\text{AlH}_6$  were calculated using both the PBE functional and the LDA.

The Brillouin zone was sampled using  $4 \times 4 \times 3$  k-point grids. Tests with up to  $7 \times 7 \times 5$  grids showed that with a  $4 \times 4 \times 3$  grid the total energy is converged to within 1.5 meV.

The resulting lattice parameters, bulk modulus and Wyckoff positions of atoms for pure  $\text{Na}_3\text{AlH}_6$  are listed in Table 1, together with experimental values [14,22,23]. The unit cell volume calculated with LDA is  $213 \text{ \AA}^3$ , while the PBE value is  $231 \text{ \AA}^3$ , to be compared with the experimental value of  $236.3 \text{ \AA}^3$  found by Gross et al. [22] at  $175 \text{ }^\circ\text{C}$ , and the values of  $229.6 \text{ \AA}^3$  and  $229.8 \text{ \AA}^3$  found by Ronnebro et al. [23] and Ozolins et al. [14] for  $\text{Na}_3\text{AlD}_6$  at room temperature, respectively. The

theoretical values we have derived do not include zero point and room temperature thermal expansion, which for  $\text{Na}_3\text{AlH}_6$  would increase the equilibrium volume by  $\sim 6.5\%$  [16], increasing our calculated LDA and PBE equilibrium volumes to  $226.7 \text{ \AA}^3$  and  $245.9 \text{ \AA}^3$  respectively [31]. The usual trend of LDA to overestimate the bulk modulus and underestimate the lattice parameters is apparent. Overall the calculated structural parameters values are in agreement with other theoretical [11–21] and experimental [14,22,23] values reported in literature.

We find an enthalpy of formation of  $-1.822 \text{ eV}$  per f.u. for bulk  $\text{Na}_3\text{AlH}_6$ , in agreement with the values of  $-1.796 \text{ eV}$  and  $-1.784 \text{ eV}$  previously reported in literature [11,32]. Before comparing this number with experiments, it is useful to compute the zero point energy (ZPE) correction to the enthalpy of formation, which can be obtained by calculating the phonons of  $\text{Na}_3\text{AlH}_6$ , Al and Na bulk. The calculations were performed with the PHON code, which employs the small displacement method [33]. We constructed supercells including 80 and 360 atoms ( $2 \times 2 \times 1$  and  $3 \times 3 \times 2$ ) for  $\text{Na}_3\text{AlH}_6$ , 64 and 125 atoms ( $4 \times 4 \times 4$  and  $5 \times 5 \times 5$ ) for both Al and Na. The reason for repeating the calculations with two supercells of different size was to check for convergence of the force constant matrix. The size of the displacements were  $0.04 \text{ \AA}$  for  $\text{Na}_3\text{AlH}_6$  and Al, and  $0.4 \text{ \AA}$  for Na, and were carefully chosen in order to ensure linearity between forces and displacements. With these prescriptions, the ZPE of the three crystals are converged to better than  $2 \text{ meV/f.u.}$  for  $\text{Na}_3\text{AlH}_6$ , and a fraction of  $1 \text{ meV/atom}$  for both Na and Al. We obtained  $E_{\text{Na}_3\text{AlH}_6}^{\text{ZPE}} = 1.153 \text{ eV}$ ,  $E_{\text{Na}}^{\text{ZPE}} = 0.017 \text{ eV}$  and  $E_{\text{Al}}^{\text{ZPE}} = 0.038 \text{ eV}$ , close to values computed by other researchers [16,34]. For the ZPE of

**Table 1 – Optimized structural parameters ( $a, b, c, \beta$  and unit cell volume  $V_0$ ), bulk modulus ( $k_0$ ), and Wyckoff positions ( $x, y, z$ ) for  $\text{Na}_3\text{AlH}_6$  calculated using both LDA and PBE, and compared to experimental values. Wyckoff positions of all listed atoms are for the 4e site. For Al(2a) and Na(2b) they are respectively (0.0,0.0,0.0) and (0.0,0.0,0.5). The calculations do not include zero point motion.**

	$a$ (Å)	$b$ (Å)	$c$ (Å)	$\beta$ (deg)	$V_0$ (Å <sup>3</sup> )	$k_0$ (GPa)
LDA	5.220	5.427	7.520	89.99	213.0	34.5
PBE	5.372	5.559	7.738	89.87	231.0	29.8
[Expt.]	[5.402, <sup>a</sup> 5.454, <sup>b</sup> 5.390 <sup>c</sup> ]	[5.507, <sup>a</sup> 5.547, <sup>b</sup> 5.514 <sup>c</sup> ]	[7.725, <sup>a</sup> 7.811, <sup>b</sup> 7.725 <sup>c</sup> ]	[89.49, <sup>a</sup> 89.83, <sup>b</sup> 89.86 <sup>c</sup> ]	[229.8, <sup>a</sup> 236.3, <sup>b</sup> 229.6 <sup>c</sup> ]	
Wyckoff positions						
	Atom	x	y	z		
LDA	Na	-0.011	0.451	0.253		
	H	0.103	0.050	0.219		
	H	0.223	0.329	0.545		
	H	0.162	0.271	0.935		
PBE	Na	-0.010	0.454	0.253		
	H	0.101	0.048	0.216		
	H	0.230	0.329	0.544		
	H	0.162	0.265	0.936		
[Expt.] <sup>a</sup>	Na	[-0.006]	[0.461]	[0.252]		
	H	[0.091]	[0.041]	[0.215]		
	H	[0.234]	[0.328]	[0.544]		
	H	[0.165]	[0.266]	[0.944]		

a Ref. [14].  $\text{Na}_3\text{AlD}_6$  at room temperature.

b Ref. [22].  $\text{Na}_3\text{AlH}_6$  at  $175 \text{ }^\circ\text{C}$ .

c Ref. [23].  $\text{Na}_3\text{AlD}_6$  at room temperature.

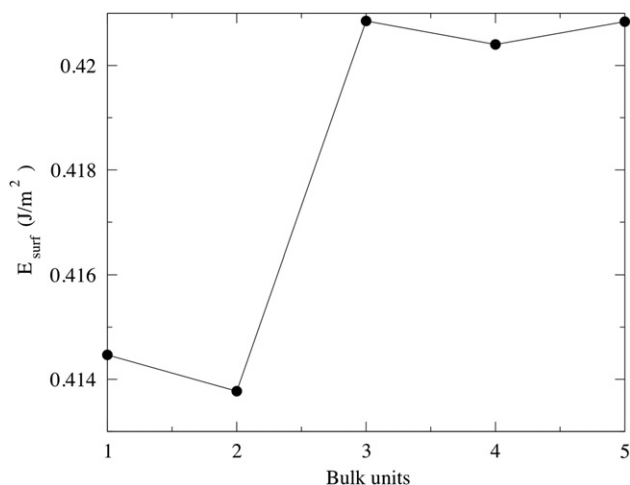


**Fig. 2 – Surface formation energy of  $\text{Na}_3\text{AlH}_6$  as a function of the number of bulk units (BUs) included in the slab.**

the  $\text{H}_2$  molecule we used the value  $E_{\text{H}_2}^{\text{ZPE}} = 0.263$  eV computed in Ref. [37]. The ZPE corrected enthalpy of formation of  $\text{Na}_3\text{AlH}_6$  is therefore  $-1.547$  eV. The discrepancy with the experimental value of  $-2.21$  eV [35,36] is probably due to inaccuracies of the PBE functional, and could be reduced with the use of more accurate electronic structure methods like quantum Monte Carlo [37,38].

### 3.1.2. Surface properties

The 010 surface has been modeled using 1, 2, 3, 4 and 5 bulk units (BUs) ( $1 \times 1 \times 1$ ,  $1 \times 2 \times 1$ ,  $1 \times 3 \times 1$ ,  $1 \times 4 \times 1$  and  $1 \times 5 \times 1$  slabs respectively), and a vacuum thickness of 16.7 Å, corresponding to three BUs. This is large enough that interactions between periodic images of the slab are completely negligible. We used  $4 \times 4 \times 4$  k-point grids to sample the surface Brillouin zone. All atoms in the simulation cell were allowed to relax.

The surface formation energy is defined as the energy per unit area required to form a surface from a bulk crystal. In a slab calculation, this can be evaluated as  $E_{\text{surf}}(N) = 1/2A [E_{\text{slab}}(N) - NE_{\text{bulk}}]$ , where  $E_{\text{slab}}(N)$  is the energy of a slab of  $N$  layers,  $E_{\text{bulk}}$  the energy of the bulk and  $A$  is the area of the surface. The factor of 1/2 comes in because a slab has two surfaces. The surface energy  $E_{\text{slab}}(N)$  depends on the number

of layers  $N$  in the slab, and therefore it needs to be evaluated in the limit of large  $N$ . However, if the bulk energy  $E_{\text{bulk}}$  is obtained from a separate bulk calculation, then  $E_{\text{surf}}(N)$  may not converge because small non-canceling errors between  $E_{\text{slab}}(N)$  and  $NE_{\text{bulk}}$ , due to non-equivalent k-point sampling, will simply grow with  $N$ . Since for large values of  $N$ ,  $E_{\text{slab}}(N)$  is proportional to  $N$ , the right procedure to obtain a converging  $E_{\text{surf}}(N)$  is to evaluate also the bulk energy from a slab calculation, or in other words fit  $E_{\text{slab}}(N)$  to a straight line and obtain  $E_{\text{bulk}}$  and  $E_{\text{surf}}$  from the slope and the intercept respectively. In doing the fit of course one needs to discard the values for the lowest value of  $N$  for which the linear dependence of  $E_{\text{slab}}(N)$  on  $N$  has not yet been obtained.

In Fig. 2 we show the surface formation energy as a function of the number of BUs included in the slab, obtained by fitting to a straight line only the energies of the  $1 \times 3 \times 1$ ,  $1 \times 4 \times 1$  and  $1 \times 5 \times 1$  slabs. It is clear that convergence to less than  $0.001$  J/m<sup>2</sup> is obtained when 3 or more BUs are included in the slab. This is because with 3 or more BUs the central BU is well converged to its bulk geometry, but with 2 or 1 each BU is obviously a surface unit. The calculated 010 surface formation energy is  $0.421$  J/m<sup>2</sup>. The geometry of the central units of the slabs is also well converged when 3 or more BUs are included. In fact, freezing the internal BU to the bulk geometry in the  $1 \times 3 \times 1$  slab increases the total energy of the slab by 0.02 eV, which would change the estimate of the surface energy by only  $0.003$  J/m<sup>2</sup>. This confirms that the  $1 \times 3 \times 1$  slab is thick enough to be able to represent bulk behavior at its center. The geometry of the outer BU is significantly affected by the presence of the vacuum (see Fig. 1), and the relaxation of the surface reduces the formation energy by  $0.21$  J/m<sup>2</sup>. In particular, the Al–H distances in the surface  $\text{AlH}_6$  complexes range between 1.69 and 1.87 Å, with the shorter distances corresponding to the two hydrogens sticking out of the surface. The corresponding distances in the bulk are 1.77–1.78 Å.

The 100 surface is more problematic: leaving the slabs free to relax causes collective rotations of the  $\text{AlH}_6$  complexes that extend to all depths of slabs of any thickness, making impossible to converge to bulk behavior in the center of the slabs. In this case the only way to reproduce bulk behavior is to freeze the geometry of the internal BUs. By doing so, we found that the surface formation energy of the 100 surface is  $0.3$  J/m<sup>2</sup> higher than that of the 010 surface, and therefore we decided to study only the latter.

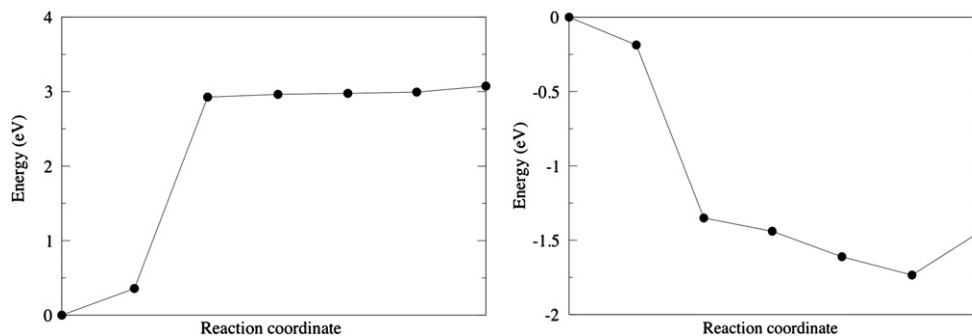


**Fig. 3 – MEP for the desorption of hydrogen from the  $\text{Na}_3\text{AlH}_6$  surface. Left panel: one H atom is removed from the surface. Right panel: a surface H atom is removed in presence of an additional H atom in the gas phase (see text).**

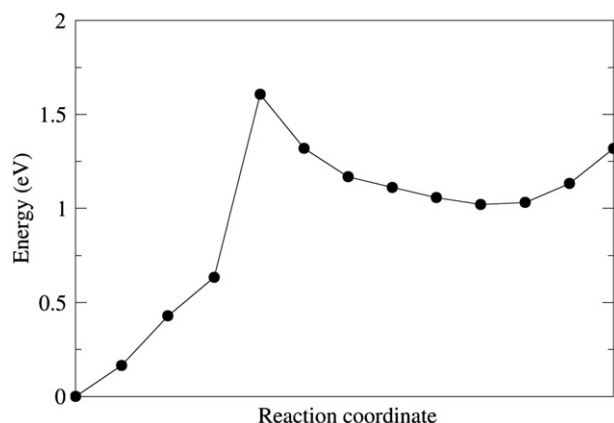


**Fig. 4** – MEP for the desorption of two H atoms from a surface  $\text{AlH}_6$  complex of the  $\text{Na}_3\text{AlH}_6$  surface, to form a  $\text{H}_2$  molecule in vacuum.

### 3.1.3. Hydrogen desorption

The binding energy of hydrogen to the  $\text{Na}_3\text{AlH}_6$  (010) surface can be calculated by removing one hydrogen from a surface  $\text{AlH}_6$  complex and placing it in vacuum. To perform this calculation, we constructed a  $2 \times 3 \times 2$  slab (12 BU units, 240 atoms), and displaced one H atom from a surface  $\text{AlH}_6$  complex  $5 \text{ \AA}$  into the vacuum. We checked that the removal energy was converged with respect to the displaced distance by moving the H atom up to  $8 \text{ \AA}$ , which showed an energy difference of less than  $2 \text{ meV}$ . The calculations were performed allowing spin polarization, which is necessary to correctly describe the hydrogen atom away from the surface. As a result of the H removal, the energy of the system increases by  $3.074 \text{ eV}$ . If referred to the energy of formation of the hydrogen molecule of  $-4.511 \text{ eV}$ , then hydrogen desorption is endothermic, with each  $\text{H}_2$  needing  $1.635 \text{ eV}$  to desorb. If two H atoms are removed from the same surface  $\text{AlH}_6$  complex, then the surface is further destabilized, and the desorption energy is reduced to  $1.32 \text{ eV}$ .

To investigate the possible presence of an energy barrier for the desorption of one hydrogen atom, we have performed two climbing-image nudged-elastic-band (NEB) calculations [39]. In the first case we considered the  $\text{Na}_3\text{AlH}_6$  slab and

removed one of the surface H atoms into the vacuum by a distance of  $5 \text{ \AA}$ . The whole system was allowed to relax along the most efficient minimum energy path (MEP). This is displayed in the left panel of Fig. 3, and shows that the hydrogen needs to climb an energy of about  $3 \text{ eV}$  to be removed from the surface, with no additional barrier to desorption. The NEB calculations shown in Fig. 3 have been performed using 7 images. We also repeated the calculations using 21 images, and found essentially the same MEP. This high energy barrier shows that it is unlikely that dehydrogenation process may proceed with a sequence of isolated H desorption events.

In the second case the initial state was that of the fully relaxed slab plus one H atom at a distance of  $5 \text{ \AA}$  from the surface, and the final state that of a fully relaxed slab with one H missing, and a hydrogen molecule in vacuum at  $5 \text{ \AA}$  from the surface. As in the previous case, the whole system was allowed to relax along the MEP. This is displayed in the right panel of Fig. 3. In this case the extra hydrogen atom comes close to the surface and collects its companion from the slab, for a desorption with no energy barrier. Before desorbing, the newly formed hydrogen molecule has a small binding energy of  $0.3 \text{ eV}$ . This shows that in the presence of atomic hydrogen in the gas phase the desorption of further hydrogen from the surface is barrier-less and exothermic, and provides a possible mechanism for the release of further hydrogen from the hexahydride by exposing it to an atmosphere of atomic hydrogen.

Finally, we have performed a third NEB calculation in which we have allowed two hydrogen atoms from a  $\text{AlH}_6$  surface cluster to desorb and form a hydrogen molecule in the vacuum. The MEP for this reaction is displayed in Fig. 4, and shows that there is a barrier of  $1.61 \text{ eV}$  for the desorption of the molecule. This is much lower than the barrier for atomic H desorption and shows that, unless atomic hydrogen is available in the gas phase, this is the mechanism that leads to the dehydrogenation of the system.

## 3.2. Ti-doped $\text{Na}_3\text{AlH}_6$

### 3.2.1. Bulk properties

We now come to the description of the Ti-doped  $\text{Na}_3\text{AlH}_6$  system. In the bulk, there are two possible Na sites and one Al site which can be substituted for Ti. Ti may also substitute

**Table 2** – Optimized structural parameters and bulk modulus for Ti-doped  $\text{Na}_3\text{AlH}_6$ , with Ti substituting for Al, Na(2b) and Na(4e) atoms.

	$a$ ( $\text{\AA}$ )	$b$ ( $\text{\AA}$ )	$c$ ( $\text{\AA}$ )	$\beta$ (deg)	$V$ ( $\text{\AA}^3$ )	$k_0$ (GPa)
Ti $\rightarrow$ Al						
$1 \times 1 \times 1$ (20 atoms)	5.468	5.618	7.869	90.06	241.7	28.9
$2 \times 1 \times 2$ (80 atoms)	5.393 (5.395) <sup>a</sup>	5.581 (5.564) <sup>a</sup>	7.771 (7.753) <sup>a</sup>	89.89 (89.98) <sup>a</sup>	233.9 (232.73) <sup>a</sup>	30.0
Ti $\rightarrow$ Na(2b)						
$1 \times 1 \times 1$ (20 atoms)	5.304	5.316	7.675	90.01	216.4	40.5
$2 \times 1 \times 2$ (80 atoms)	5.349 (5.343) <sup>a</sup>	5.535 (5.463) <sup>a</sup>	7.707 (7.635) <sup>a</sup>	89.92 (89.81) <sup>a</sup>	228.2 (223.26) <sup>a</sup>	30.9
Ti $\rightarrow$ Na(4e)						
$1 \times 1 \times 1$ (20 atoms)	5.331	5.671	7.498	89.14	225.7	22.9
$1 \times 1 \times 1$ (80 atoms)	5.357	5.544	7.719	89.89	229.3	27.8

a From theoretical calculations of Li et al., 2006 [18].

**Table 3 – Substitution enthalpies of Ti-doped Na<sub>3</sub>AlH<sub>6</sub>, calculated with ( $\Delta H^{\text{spin}}$ ) and without ( $\Delta H$ ) spin-polarizations. Slab results are calculated using a  $2 \times 3 \times 2$  supercell and a vacuum thickness of 16.7 Å, bulk results using a  $2 \times 1 \times 2$  supercell. Al, Al<sub>2</sub> and Al<sub>3</sub> refer to the Al site in the first, second and third layer of the slab. For the bulk all the Al sites are equivalent. Na and Na<sub>2</sub> refer to the (4e) and (2b) Na sites in the first layer respectively, Na<sub>3</sub> and Na<sub>4</sub> to the corresponding sites in the second layer, and Na<sub>5</sub> and Na<sub>6</sub> to those in the third layer. Note the significant stabilizing effect of the inclusion of spin polarization in the calculations.**

Ti → Al/Na	$\Delta H$ (eV)	$\Delta H^{\text{spin}}$ (eV)	$\Delta H_{\text{Bulk}}$ (eV)	$\Delta H_{\text{Bulk}}^{\text{spin}}$ (eV)
Al	0.589	0.343		
Al <sub>2</sub>	0.803	0.549		
Al <sub>3</sub>	0.952	0.732	0.975 (0.93, <sup>a</sup> 0.95 <sup>b</sup> )	0.753
Na	1.029	0.788		
Na <sub>2</sub>	1.011	0.731		
Na <sub>3</sub>	1.542	1.050		
Na <sub>4</sub>	2.098	1.207		
Na <sub>5</sub>	1.770	1.583	2.059 (2.00 <sup>b</sup> )	1.837
Na <sub>6</sub>	2.487	1.576	2.435 (2.42, <sup>a</sup> 2.44 <sup>b</sup> )	1.507

a Ref. [18].  
b Ref. [20].

interstitially, but it was found by Lee et al. [19] that these sites are unfavorable, and for this reason we did not include them in our study.

The energetics, structural and electronic properties of Ti-doped bulk Na<sub>3</sub>AlH<sub>6</sub> systems have been investigated by Li et al. [18], who found that the Al site is the most stable site for Ti, and that the hydrogen–metal distances increase from 1.76 Å in the AlH<sub>6</sub> complex in the pure system to 1.85 Å in the TiH<sub>6</sub> complex when Ti is substituted for a Al atom, while the Ti–H distances increase to 1.99 Å when Ti is substituted for a Na atom. They also found that the volume of their 80 atoms supercell increased slightly when one Ti atom was substituted for a Al atom, and that the geometry of the system is only affected locally by Ti. By contrast, the equilibrium volume of the system is slightly reduced when the Ti atom is substituted for a Na atom.

Similarly, here we have studied the structural parameters of Ti-doped bulk Na<sub>3</sub>AlH<sub>6</sub>. We optimized both atomic coordinates and cell shape, using the PBE functional only. The structural parameters were determined by fitting energy versus volume curves to a Birch–Murnaghan equation of state [30]. We studied the Ti-doped systems both at high (20 atoms) and low (80 atoms) Ti concentration.

Table 2 lists the optimized lattice parameters and bulk modulus for Ti-doped Na<sub>3</sub>AlH<sub>6</sub>, when substituting at Al, Na(2b) and Na(4e) atomic sites. In agreement with Li et al. [18], we find that when Ti substitutes for an Al atom the unit cell volume increases, while it decreases when Ti is substituted for a Na atom. The volume effect is obviously bigger on the smaller 20 atoms cell. We also note that spin polarization is necessary to obtain accurate substitution enthalpies (see below), although the effect on the structural properties is small. We find that the Ti–Al distances in the TiH<sub>6</sub> complex increase to 1.86–1.87 Å

when Ti is substituted for a Al atom, while they are between 1.99 and 2.01 Å when Ti is substituted for a Na atom. These values agree well with those found by Li et al. [18].

### 3.2.2. Surface properties

To study the Ti-doped surface we used a  $2 \times 3 \times 2$  slab, as in the pure case, which contains a total of 12 bulk units, or 240 atoms. All the atoms in the simulation cell were allowed to relax. In this slab there are 3 and 6 non-equivalent Al and Na sites, respectively (see details in caption of Table 3). The substitution enthalpies of the doped systems are calculated according to:

$$\Delta H = E(\text{TiNa}_{72-x}\text{Al}_{24-y}\text{H}_{144}) - E(\text{Na}_{72}\text{Al}_{24}\text{H}_{144}) - E(\text{Ti}) + xE(\text{Na}) + yE(\text{Al}) \quad (4)$$

where  $E(\text{TiNa}_{72-x}\text{Al}_{24-y}\text{H}_{144})$  is the energy of the slab in which one Na or one Al atom has been replaced by a Ti atom,  $E(\text{Ti})$ ,  $E(\text{Na})$  and  $E(\text{Al})$  are the energies of Ti, Na and Al bulk, respectively, and  $x$  and  $y$  are integers equal to 1 or 0, with  $x + y = 1$ .

We report the values of  $\Delta H$  for the 9 sites in Table 3. We also report the values of  $\Delta H$  for the bulk, from which we see that in agreement with Li et al. [18] the Al sites are those with the lowest substitution enthalpies. The calculations were performed by allowing spin polarization, which is essential to describe the magnetic moments localized on the Ti atom (with values of about 1  $\mu_B$  and above) and stabilizes the doped crystal significantly. We also notice that the substitution enthalpies of the sites in the center of the slab are very close to those calculated for the bulk, further confirming that the center of the slab is indeed bulk-like.

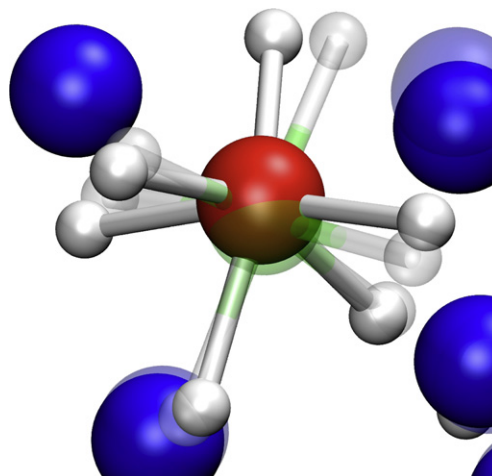


**Fig. 5 – Geometry of the relaxed TiNa<sub>72</sub>Al<sub>23</sub>H<sub>144</sub> slab near the Ti atom. Na, Al and H atoms are shown as blue (dark gray), green (light gray) and small white balls respectively, Ti atom is shown in red. Also shown are the corresponding positions of the pure Na<sub>72</sub>Al<sub>24</sub>H<sub>144</sub> slab (shadowed balls). (For interpretation of the references to color in this figure legend, the reader is referred to the web version of this article.)**

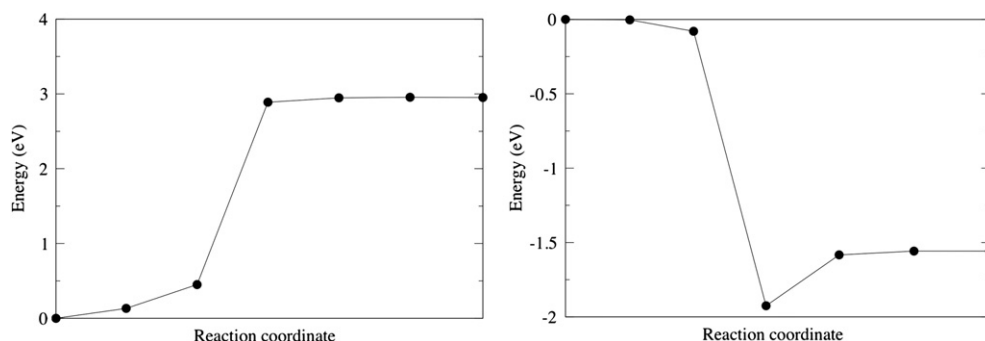


**Fig. 6** – MEP for the desorption of hydrogen from the  $\text{TiNa}_{72}\text{Al}_{23}\text{H}_{144}$  slab. Left panel: only one H atom is removed from the surface. Right panel: a surface H atom is removed in presence of an additional H atom in the gas phase (see text).

Interestingly, the substitution enthalpies are much smaller when Ti is substituted for a surface atom, which means that Ti atoms will be localized on the surface at low temperature. In fact, since the enthalpy difference between surface and bulk sites is of the order of 0.4 eV, the segregation energy will remain negative (i.e. favor surface sites) to temperatures much higher than room temperature, and therefore the Ti atoms will remain localized on the surface even at moderately high temperatures.

Given the significantly lower value of  $\Delta H$  for the Al surface site compared to both Na surface sites, we restricted our investigation to this particular site only. As for the bulk, we observe that the Ti–H distances are lengthened when compared to the Al–H distances, to 1.84–1.91 Å, and the geometry of the  $\text{TiH}_6$  complex is also significantly distorted, as shown in Fig. 5. However, the distortion is localized around the Ti atom, and does not extend for more than two layers inside the bulk.

### 3.2.3. Hydrogen desorption

The hydrogen removal energy from the Ti-doped surface is 2.952 eV, which is about 0.1 eV lower than that from the pure surface, and therefore a desorption of two atoms to form an  $\text{H}_2$  molecule would be endothermic with an energy penalty of 1.393 eV, slightly lower than the 1.635 eV calculated for the pure surface. However, if two H atoms are removed from the  $\text{TiH}_6$  complex the desorption energy increases to 1.53 eV. This is slightly higher than the desorption energy on the pure system. However, as we shall see, the presence of Ti reduces the energy barrier to hydrogen desorption.

To investigate the dehydrogenation of the  $\text{TiNa}_{72}\text{Al}_{23}\text{H}_{144}$  system we performed three NEB calculations, in a similar way as described for the pure case. In the first case we removed one H atom from a surface  $\text{TiH}_6$  complex. The MEP shows that, as in the pure case, the energy increases monotonously to 2.95 eV, with no additional energy barrier (see Fig. 6). Also in this case the calculations were performed with 7 images and a check with 21 images did not show appreciable differences in the MEP.

In the second case we introduced a second H atom in the system, and as in the pure case we found that the extra H atom comes close to the surface and the desorption of the  $\text{H}_2$  molecule proceeds with no energy barrier. As in the pure case,

we observe that before desorbing the newly formed hydrogen molecule has a small binding energy of 0.37 eV.

The third calculation, in which we have allowed two hydrogen atoms from the  $\text{TiH}_6$  surface cluster to desorb and form a hydrogen molecule in the vacuum, is shown in Fig. 7. Interestingly, in this case there is no barrier to desorption, even though the final energy is slightly higher than that for a molecule desorbing from an  $\text{AlH}_6$  complex. This clearly shows that Ti doping can be beneficial, by improving the kinetics of the desorption process.

### 3.3. Electronic structure

The electronic structure of both pure and Ti-doped  $\text{Na}_3\text{AlH}_6$  has been investigated by previous authors [14–16,18]. In this section we revisit the issue, mainly to highlight the effect of the introduction of spin polarization in the calculations for the Ti-doped system. In Fig. 8 we show the total and the partial density of states (PDOS) of bulk  $\text{TiNa}_{24}\text{Al}_7\text{H}_{48}$  and the  $\text{TiNa}_{72}\text{Al}_{23}\text{H}_{144}$  slab. For the bulk we also calculated the PDOS for the  $\text{TiNa}_{72}\text{Al}_{23}\text{H}_{144}$  system, which showed no appreciable differences with the system with a larger concentration of Ti. The PDOS have been obtained by projecting the Kohn–Sham orbitals onto spherical harmonics with angular momentum 0,

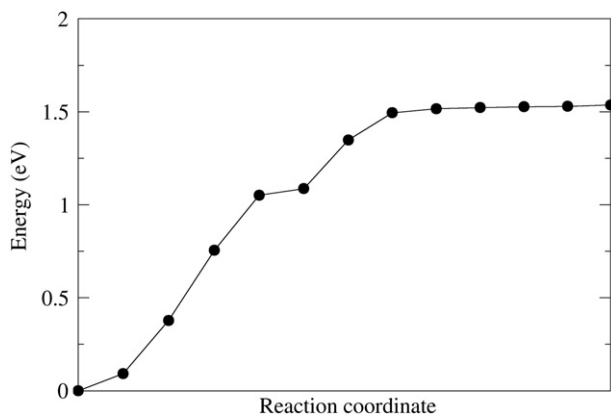


**Fig. 7** – MEP for the desorption of two H atoms from a surface  $\text{TiH}_6$  complex of the  $\text{TiNa}_{72}\text{Al}_{23}\text{H}_{144}$  slab, to form a  $\text{H}_2$  molecule in vacuum.

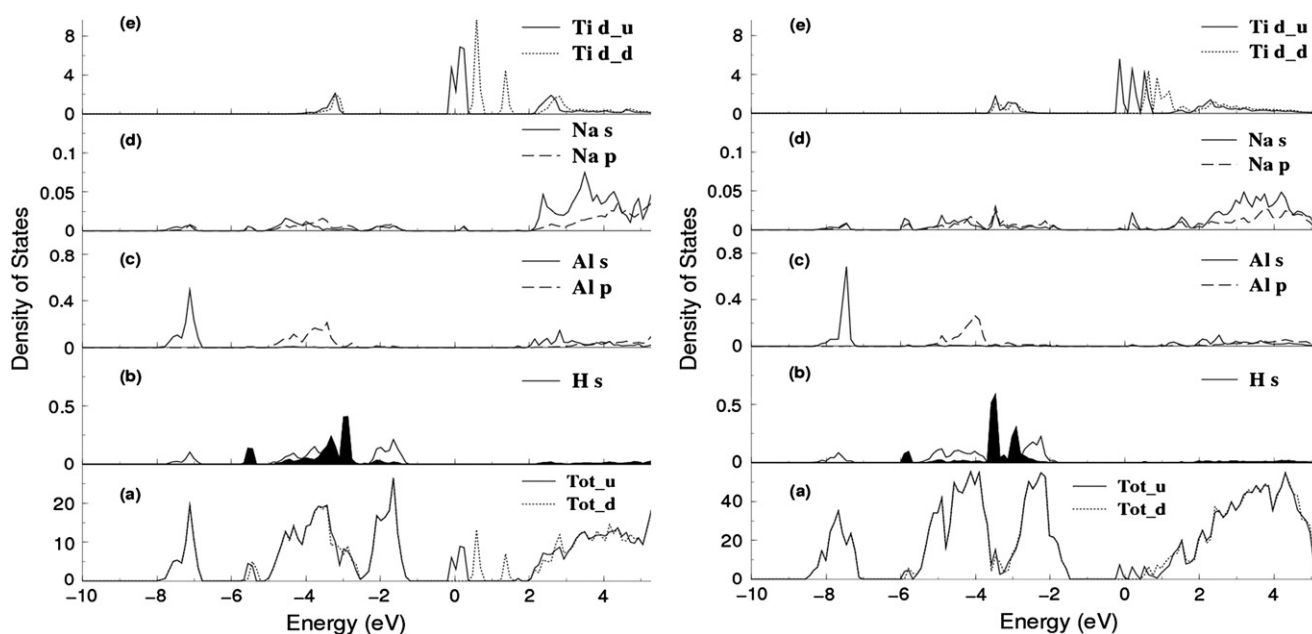


**Fig. 8** – Left panel: density of states of bulk  $\text{TiNa}_{24}\text{Al}_7\text{H}_{48}$ ; panels (a), (b), (c), (d) and (e) show the total DOS (both spin up and spin down), the s-PDOS of the H atoms (in black one of the H atoms near a Ti atom), the s- and p-PDOS of Al, the s- and p-PDOS of Na and the d-PDOS of Ti (both for spin up and spin down) respectively. The spin up and spin down components of the PDOS of H, Al and Na are indistinguishable and therefore only one component is plotted. Right panel: analogous quantity for the  $\text{TiNa}_{72}\text{Al}_{23}\text{H}_{144}$  slab, with the Ti atom on the surface.

1 and 2 (s, p, and d), inside spheres centered around the atoms. The radii of the spheres were 1.16, 1.32, 1.40 and 0.37 Å for Na, Ti, Al and H respectively. It is clear that there are only very small differences between the surface and the bulk PDOS, as expected for an ionic crystal.

The two spin components of the projections are essentially identical for H, Al and Na, and therefore in Fig. 8 we only show one of the two. The projections onto the Ti atom, however, are different, showing a splitting of the Ti d-PDOS around the Fermi energy, which is the cause of the insurgence of a magnetic moment localized on the Ti atom.

The resonance between the Ti  $e_g$  orbitals and the H 1s orbitals can be interpreted as a sign of covalent bonding between Ti and H [11,18].

The ionicity of the crystal, and a slight change in ionicity in the region around the Ti atom in the doped crystal, is also confirmed by an analysis of the Bader charges [40,41]. For the pure  $\text{Na}_3\text{AlH}_6$  system we find that the Na atoms donate 0.8–0.85 electrons (e), the Al atoms donate approximately 2.2e, and the H atoms gain approximately 0.78e. The charge distribution is hardly affected by the presence of the surface, in support of the discussion on the electronic density of states.

For the  $\text{TiNa}_{72}\text{Al}_{23}\text{H}_{144}$  system the only differences to be found are in the Bader charges of the H atoms in the  $\text{TiH}_6$  complex. Here the ionicity of the H atoms is slightly reduced from  $\sim 0.78e$  to  $\sim 0.65e$ , because the Ti atom only donates  $\sim 1.35e$ , in contrast to the  $\sim 2.2e$  donated by the Al atoms. The surface is also found to affect the Bader charges only marginally, with just  $\sim 0.05$  fewer electrons donated by Ti to

the surrounding H atoms. The lower ionicity of the  $\text{TiH}_6$  complex compared to the  $\text{AlH}_6$  complex could explain why the doped surface releases hydrogen more easily.

#### 4. Conclusions

We have studied the dehydrogenation properties of both pure and Ti-doped  $\text{Na}_3\text{AlH}_6$  systems, investigating in particular the role of the surface in the desorption of hydrogen. We found that for both the pure and the Ti-doped systems, atomic H desorption has a large energy barrier (3.07 and 2.95 eV for the pure and the Ti-doped systems, respectively), showing that this mechanism towards dehydrogenation is unlikely. A process with a lower energy barrier is that of molecular hydrogen desorption, with two H atoms detaching from the same surface  $\text{AlH}_6$  or  $\text{TiH}_6$  complexes. For the pure system,  $\text{H}_2$  desorption from a surface  $\text{AlH}_6$  complex is endothermic, with an energy penalty of 1.32 eV, and has an energy barrier of 1.61 eV. For the doped system,  $\text{H}_2$  desorption from a  $\text{TiH}_6$  complex is also endothermic, with a higher energy penalty of 1.53 eV, but there is no energy barrier, and therefore the kinetics of desorption should be improved as a result.

On both the pure and the Ti-doped surfaces the most efficient desorption process would be the one assisted by the presence of atomic hydrogen in the gas phase, which is barrier-less and exothermic.

By calculating the substitution enthalpy of Ti in various sites, we confirmed that between Al and Na the preferred sites are the Al ones. We found that the segregation energy is

negative, and therefore Ti atoms will be localized on the surface. We also found that the Ti atom in the hexahydride carries a magnetic moment, and therefore allowing spin polarization in the calculations has the effect of reducing the energy of the doped systems, increasing its stability compared to what previously reported. This means that it is not so unfavourable for Ti to dissolve in the surface, and kinetics may allow it to remain in this metastable configuration for long time, particularly if the dopant concentration is low, and stability is helped by entropy. However, because of the positive enthalpy of formation, it is possible that for sufficiently large concentrations Ti clusters will form on the surface, and therefore it will be interesting in future work to investigate the effect of doping  $\text{Na}_3\text{AlH}_6$  with small Ti clusters, which were found to be beneficial in  $\text{NaAlH}_4$  [9]. It will be also interesting to study the properties of the hexahydride doped with different transition metals or even Ce, which was found to improve the kinetics of  $\text{NaAlH}_4$  [8].

## Acknowledgments

This work was conducted as part of a EURYI scheme award as provided by EPSRC (see [www.esf.org/euryi](http://www.esf.org/euryi)). The calculations were run on the UK national facility HECToR and on the UCL facility Legion. We greatly acknowledge useful discussion with A. Amieiro and M. Sarwar.

## REFERENCES

- [1] Sakintuna B, Lamari-Darkrim F, Hirscher M. Metal hydride materials for solid hydrogen storage: a review. *Int J Hydrogen Energy* 2007;32(9):1121–40.
- [2] Bogdanović B, Schwickardi M. Ti-doped alkali metal aluminium hydrides as potential novel reversible hydrogen storage materials. *J Alloys Compd* 1997;253–254:1–9.
- [3] Jensen CM, Zidan R, Mariels N, Hee A, Hagen C. Advanced titanium doping of sodium aluminum hydride: segue to a practical hydrogen storage material? *Int J Hydrogen Energy* 1999;24(5):461–5.
- [4] Jensen CM, Gross KJ. Development of catalytically enhanced sodium aluminum hydride as a hydrogen-storage material. *Appl Phys A Mater Sci Process* 2001;72(2):213–9.
- [5] Ashby EC, Kobetz P. The direct synthesis of  $\text{Na}_3\text{AlH}_6$ . *Inorg Chem* 1966;5(9):1615–7.
- [6] Zidan RA, Takara S, Hee AG, Jensen CM. Hydrogen cycling behavior of zirconium and titanium–zirconium-doped sodium aluminum hydride. *J Alloys Compd* 1999;285(1–2):119–22.
- [7] Kircher O, Fichtner M. Kinetic studies of the decomposition of  $\text{NaAlH}_4$  doped with a Ti-based catalyst. *J Alloys Compd* 2005;404–406:339–42.
- [8] Léon A, Rothe J, Chlopek K, Zabara O, Fichtner M. Fluorescence XAFS study of  $\text{NaAlH}_4$  doped with a Ce-based precursor. *Phys Chem Chem Phys* 2009;11(39):8829–34.
- [9] Fichtner M, Fuhr O, Kircher O, Rothe J. Small Ti clusters for catalysis of hydrogen exchange in  $\text{NaAlH}_4$ . *Nanotechnology* 2003;14(7):778–85.
- [10] Pozzo M, Alfè D. Hydrogen dissociation and diffusion on transition metal (=Ti, Zr, V, Fe, Ru, Co, Rh, Ni, Pd, Cu, Ag)-doped Mg(0001) surfaces. *Int J Hydrogen Energy* 2009;34(4):1922–30.
- [11] Opalka SM, Anton DL. First principles study of sodium–aluminum-hydrogen phases. *J Alloys Compd* 2003;356–357:486–9.
- [12] Arroyo y de Dompablo ME, Ceder G. First principles investigations of complex hydrides  $\text{AMH}_4$  and  $\text{A}_3\text{MH}_6$  ( $A = \text{Li, Na, K, M} = \text{B, Al, Ga}$ ) as hydrogen storage systems. *J Alloys Compd* 2004;364(1–2):6–12.
- [13] Íñiguez J, Yildirim T, Udovic TJ, Sulic M, Jensen CM. Structure and hydrogen dynamics of pure and Ti-doped sodium alanate. *Phys Rev B* 2004;70(6):060101(R) (4 pp.).
- [14] Ozolins V, Majzoub EH, Udovic TJ. Electronic structure and Rietveld refinement parameters of Ti-doped sodium alanates. *J Alloys Compd* 2004;375(1–2):1–10.
- [15] Peles A, Alford JA, Ma Zhu, Yang Li, Chou MY. First-principles study of  $\text{NaAlH}_4$  and  $\text{Na}_3\text{AlH}_6$  complex hydrides. *Phys Rev B* 2004;70(16):165105 (7 pp.).
- [16] Ke X, Tanaka I. Decomposition reactions for  $\text{NaAlH}_4$ ,  $\text{Na}_3\text{AlH}_6$ , and  $\text{NaH}$ : first-principles study. *Phys Rev B Condens Matter Mater Phys* 2005;71(2):024117 (16 pp.).
- [17] Vajeeston P, Ravindran P, Kjekshus A, Fjellvåg H. First-principles investigations of aluminum hydrides:  $\text{M}_3\text{AlH}_6$  ( $M = \text{Na, K}$ ). *Phys Rev B* 2005;71(9):092103 (4 pp.).
- [18] Li S, Jena P, Ahuja R. Effect of Ti and metal vacancies on the electronic structure, stability, and dehydrogenation of  $\text{Na}_3\text{AlH}_6$ : supercell band-structure formalism and gradient-corrected density-functional theory. *Phys Rev B* 2006;73(21):214107 (7 pp.).
- [19] Lee E-K, Cho YW, Yoon JK. Ab-initio calculations of titanium solubility in  $\text{NaAlH}_4$  and  $\text{Na}_3\text{AlH}_6$ . *J Alloys Compd* 2006;416(1–2):245–9.
- [20] Voss J, Shi Q, Jacobsen HS, Zamponi M, Lefmann K, Vegge T. Hydrogen dynamics in  $\text{Na}_3\text{AlH}_6$ : a combined density functional theory and quasielastic neutron scattering study. *J Phys Chem B* 2007;111(15):3886–92.
- [21] Monteferrante M, Bonella S, Meloni S, Vanden-Eijnden E, Ciccotti G. Calculations of free energy barriers for local mechanisms of hydrogen diffusion in alanates. *Sci Model Simul* 2008;15:187–206.
- [22] Gross KJ, Guthrie S, Takara S, Thomas G. In-situ X-ray diffraction study of the decomposition of  $\text{NaAlH}_4$ . *J Alloys Compd* 2000;297(1–2):270–81.
- [23] Rönnebro E, Noréus D, Kadir K, Reiser A, Bogdanovic B. Investigation of the perovskite related structures of  $\text{NaMgH}_3$ ,  $\text{NaMgF}_3$  and  $\text{Na}_3\text{AlH}_6$ . *J Alloys Compd* 2000;299(1–2):101–6.
- [24] Perdew JP, Burke K, Ernzerhof M. Generalized gradient approximation made simple. *Phys Rev Lett* 1996;77(18):3865–8.
- [25] Blöchl PE. Projector augmented-wave method. *Phys Rev B* 1994;50(24):17953–79.
- [26] Kresse G, Joubert D. From ultrasoft pseudopotentials to the projector augmented-wave method. *Phys Rev B* 1999;59(3):1758–75.
- [27] Kresse G, Furthmüller J. Efficient iterative schemes for ab initio total-energy calculations using a plane-wave basis set. *Phys Rev B* 1996;54(16):11169–86.
- [28] Alfè D. Ab initio molecular dynamics, a simple algorithm for charge extrapolation. *Comput Phys Commun* 1999;118(1):31–3.
- [29] Humphrey W, Dalke A, Schulten K. VMD: visual molecular dynamics. *J Mol Graphics* 1996;14(1):33–8.
- [30] Birch F. Finite elastic strain of cubic crystals. *Phys Rev* 1947;71(11):809–24.
- [31] The LDA equilibrium volume corrected for room temperature thermal expansion appears to be very close to the values reported in Refs. [14,23], however, these results refer to  $\text{Na}_3\text{AlH}_6$ , for which zero point and room temperature thermal expansion will obviously be lower.

- [32] Wilson-Short GB, Janotti A, Hoang K, Peles A, Van de Walle CG. First-principles study of the formation and migration of native defects in  $\text{NaAlH}_4$ . *Phys Rev B* 2009;80(22):224102 (8pp.).
- [33] Alfè D. PHON: a program to calculate phonons using the small displacement method. *Comput Phys Commun* 2009;180(12):2622–33.
- [34] Qiu C, Opalka SM, Olson GB, Anton DL. Thermodynamic modeling of the sodium alanates and the Na–Al–H system. *Int J Mat Res* 2006;97(11):1484–94.
- [35] The experimental value  $-2.21$  eV has been obtained by extrapolating to zero temperature the room temperature value of  $-2.475$  eV reported by Lee et al. [36].
- [36] Lee B-M, Jang J-W, Shim J-H, Cho YW, Lee B-J. Thermodynamic assessment of the  $\text{NaH} \leftrightarrow \text{Na}_3\text{AlH}_6 \leftrightarrow \text{NaAlH}_4$  hydride system. *J Alloys Compd* 2006;424(1–2):370–5.
- [37] Pozzo M, Alfè D. Structural properties and enthalpy of formation of magnesium hydride from quantum Monte Carlo calculations. *Phys Rev B* 2008;77(10):104103 (8pp.).
- [38] Mao G, Hu X, Wu X, Dai Y, Chu S, Deng J. Benchmark quantum Monte Carlo calculation of the enthalpy of formation of  $\text{MgH}_2$ . *Int J Hydrogen Energy* 2011;36(14):8388–91.
- [39] Mills G, Jonsson H, Schenter GK. Reversible work transition state theory: application to dissociative adsorption of hydrogen. *Surf Sci* 1995;324(2–3):305–37; Jonsson H, Mills G, Jakobsen KW. Nudged elastic band method for finding minimum energy paths of transitions. In: Berne BJ, Ciccotti G, Coker DF, editors. *Classical and quantum dynamics in condensed phase simulations*. Singapore: World Scientific; 1998. p. p385–404; Henkelman G, Jonsson H. Improved tangent estimate in the nudged elastic band method for finding minimum energy paths and saddle points. *J Chem Phys* 2000;113(22):9978–85; Henkelman G, Uberuaga BP, Jonsson H. A climbing image nudged elastic band method for finding saddle points and minimum energy paths. *J Chem Phys* 2000;113(22):9901–4.
- [40] Henkelman G, Arnaldsson A, Jonsson H. A fast and robust algorithm for Bader decomposition of charge density. *Comput Mater Sci* 2006;36(3):354–60; Sanville E, Kenny SD, Smith R, Henkelman G. Improved grid-based algorithm for Bader charge allocation. *J Comput Chem* 2007;28(5):899–908; Tang W, Sanville E, Henkelman G. A grid-based Bader analysis algorithm without lattice bias. *J Phys Condens Matter* 2009;21(8):084204 (7pp.).
- [41] Available from: <http://theory.cm.utexas.edu/bader/>.